# A spinning drop tensioextensometer

D. D. Joseph, M. S. Arney, G. Gillberg,[a] H. Hu, D. Hultman, C. Verdier,[b] and T. M. Vinagre

*Department of Aerospace Engineering and Mechanics, University of Minnesota, Minneapolis, Minnesota 55455*

Reprinted from JOURNAL OF RHEOLOGY, May 1992 

# A spinning drop tensioextensometer

D. D. Joseph, M. S. Arney, G. Gillberg,[a] H. Hu, D. Hultman, C. Verdier,[b] and T. M. Vinagre

*Department of Aerospace Engineering and Mechanics, University of Minnesota, Minneapolis, Minnesota 55455*

(Received 31 October 1991; accepted 22 February 1992)

**Synopsis**

We examine some theoretical and experimental aspects of the measurement of interfacial tension, stress relaxation in elongational flow, and yield stresses in organic liquids, blends of polymer melts, and liquid crystal polymers. This study is based on an instrument which is an improved version of the spinning drop apparatus that is commonly used to measure interfacial tension between melted polymers. Problems of vibrations at high speed, heating of the bearings, high temperatures required to melt the polymers, outgassing at the reduced pressures generated by rotation, and other problems have been eliminated in the improved apparatus. This same instrument can be used to generate curves of volume expansion versus temperature for blended systems and to detect and interpret yield stresses which occur in some polymers and strongly influence the properties of blends. The instrument has been enhanced for accurate measurements of drop diameter, length and shape as a function of time and initial conditions. A theory of upper and lower bounds for interfacial tension and a theoretically based method of exponential fitting has been developed to help to overcome the problems of slow approach to equilibrium between highly viscous melts. We have developed and propose to develop further a theory of relaxation in which transient measurements of drop diameter can be used to obtain rheological properties like elongational and yield stresses and interfacial tension and more generally to interpret the curves of relaxation generated in the experiments.

## I. INTRODUCTION

To obtain desired material properties, a blend of two incompatible polymers are often used. The properties of the polymer blend are to a

[a] Hoechst Celanese Corp., Summit, NJ.
[b] Institut de Mecanique, Grenoble, France.

large extent determined by the morphology of the blend, i.e., the size and shape of the elements of the dispersed phase and their distribution. The blend morphology developed during the mixing process of the incompatible polymers in the molten state is strongly influenced by the interfacial tension between the liquid phases. The stability of the morphology is also dependent on the viscoelasticity and the viscosity ratio of the molten polymers. Other factors affecting the polymer blend morphology are the total strain, processing time, and temperature (Wu, 1987). Wu showed that the smallest dispersed droplet size is obtained when the viscosities of the two polymers are matched and the interfacial tension is low. Later studies reported by Shih (1991) have shown that a phase inversion will take place during the blending if the continuous phase in the final blend has a higher melting temperature than the dispersed phase. The addition of appropriate dispersants or compatibilizers can reduce the interfacial tension significantly.

Commonly used compatibilizers are diblock copolymers, each block having a composition similar to one of the polymer phases. In addition to reducing the interfacial tension they also improve the adhesion between the two phases (Xanthos, 1988; Gaylord, 1989). Ideally all added compatibilizer should migrate to the interface during the blending operation. Several characterization techniques exist to determine the location of the compatibilizer in the final blend, e.g., electron microscopy, SEM and TEM of stained samples, nonradiative energy transfer (NRET) using labeled polymers, thermal transition analysis (differential scanning calorimetry and thermally stimulated depolarization currents), and solid state NMR (Fayt *et al.*, 1987). Optimization processes today involve the synthesis of the compatibilizer and evaluating its effect on the final blend, often implying time consuming feedback cycles. This optimization process could be simplified if a method to evaluate the effect of the compatibilizers on the interfacial tension of the polymer melts as a function of time were available.

Several methods have been used to study the interfacial tension of polymers. They are all based on the measurement of droplet profiles. Because of the high viscosity of most commercial polymers, equilibrium profiles are obtained only after long times with the risk of thermal degradation of the polymers. Changes in interfacial tension with time could thus be due to the establishment of equilibrium, to the formation of degradation products, or, in the case of a system containing a compatibilizer, to the diffusion of the compatibilizer to the interface.

We have developed and improved a spinning drop tensiometer for polymer melts that allow high temperatures and high rotational speeds.

The instrument yields relaxation curves for the drop parameters whose terminal asymptotic value gives the interfacial tension. By developing a guiding mathematical theory for the relaxation curves and by utilizing new concepts of upper and lower curves of relaxation and the relaxation time for the system, it should be possible to distinguish between changes in interfacial tension due to polymer chain relaxations and the effects of diffusion of possible compatibilizers to the interface. If this were to be possible it would have an important impact on our understanding of the necessary structural requirements to develop high performance systems.

## II. METHODS TO DETERMINE INTERFACIAL TENSION BETWEEN POLYMERS

The most common method is the pendent drop method in which a drop of one of the molten polymers is allowed to form in the other under influence of gravity. The technique relies on a force balance between gravitational forces and interfacial tension. In the case of viscous polymer melts it can take hours or even days for the equilibrium shape to be obtained. The polymers have to be kept in an inert (argon) atmosphere to avoid oxidative degradation. Thermal degradation is, however still, a problem (Wu, 1974; Wu, 1969; Roe, 1968; Anastasiadis *et al.*, 1986). The sessile drop method is a closely related method.

The determination of polymer interfacial tension by the capillary breakup of a fluid thread which was originally suggested by Chappelar (1964) has achieved renewed interest (Elmendorp, 1986; Carriere, Cohen, and Arends, 1989; Carriere and Cohen, 1991; Elemans, Janssen, and Meijer, 1990). The motivation for the development is expressed well in the words of the authors last named: "In contrast to the other methods for measuring interfacial tension, such as the pendent or spinning drop, the breaking thread method does not require data on the density difference between the two phases, which is often difficult to measure with sufficient accuracy. The method is also suitable for systems consisting of polymers with small density differences and for systems with extremely high viscosities where a pendent or spinning drop requires several hours to attain an equilibrium shape." [Some of these issues are also addressed by the spinning drop extensometer described here, which allows for precision measurements of density versus temperature in the same instrument, and works well and fast for polymer melts with zero shear viscosities certainly in the range between $10^5$ and $10^6$ P (see Table I) and probably higher.]

**TABLE I.** Material properties of liquids and polymers.

| Material | Temp. (°C) | $M_w$ (g/mol) | $M_n$ (g/mol) | Density (g/cm$^3$) | Zero-shear viscosity (Pa s) |
|---|---|---|---|---|---|
| 100 000 cs polydimethylsiloxane (PDMS) | 25 | | | 0.977 | 97.7 |
| 10 000 cs polydimethylsiloxane (PDMS) | 25 | | | 0.975 | 9.75 |
| Glycerol | 25 | | | 1.255 | 0.69 |
| Low density polyethylene (LDPE) | 200 | 253 000 | 52 000 | 0.761 | 32 000 |
| Polymethylmethacrylate (PMMA) | 200 | 85 000 | 47 000 | 1.092 | 38 000 |
| Polystyrene (PS) | 200 | 294 000 | 122 000 | 0.985 | 50 000 |

There are two different capillary thread methods being used: the embedded fiber retraction method (IFR) used by Carriere *et al.* and the breaking thread method used by everyone else. These two methods could be called the method of short and long threads, respectively. Both methods involve following the change in shape of a fiber embedded in a polymer matrix when the polymers are molten. In both cases, sample preparations are laborious, and the thread and the matrix must be relieved of residual stresses. Both methods are dynamic since there is no equilibrium near to a thread, long or short. In the short thread method the retraction of the thread into a sphere, which is an equilibrium shape far from a thread, is monitored. This method uses zero shear rate viscosities of the phases, not the density difference. The interfacial tension is calculated using the time required for retraction into a sphere and the radius of the sphere. The interfacial tension is directly proportional to the sphere radius and inversely proportional to the retraction time. An approximate Newtonian theory has been used, with inertia, elastic effects, and gravity neglected, and the true geometry of contraction is represented by what are called effective values.

The long thread, or breaking thread method, does not use thread breakup but instead concentrates on the early stages of thread deformation in which it is supposed that the purely viscous theory of Tomotika (1935) applies. Elastic and gravity effects are neglected. The neglecting of gravity could be important when the density difference between polymers is not negligible. Elmendorp (1986) noted that Newtonian behavior was evident only in the initial stages of thread breakup. Elemans *et*

*al.* (1990) indicated that the thread method needs an initially uniform long thread and that this requirement is more readily achieved when the thread viscosity is larger than the matrix viscosity. Only data on pairs of polymers satisfying this viscosity condition were reported. Carriere and Cohen (1991) gave some criticisms of the long thread technique based on their experience. They noted that, besides the restrictions on the applicability of the method already mentioned, "...Difficulties related to the effective encapsulation of long fibers by the matrix, its alignment, problems of air entrapment, and fiber distortions provide severe obstacles for successful experimentation." They further note that retraction of the long fiber which occurs in experiments is not considered in the theory. It is perhaps useful to note that fiber methods could not easily be made to work for the interfacial tension of mobile liquids of low viscosity.

In the spinning drop method a drop of the less dense polymer melt is placed in the melt of the polymer of higher density contained in a horizontal tube. The tube is spun at a constant speed. For each speed of rotation, the drop will attain an equilibrium shape which is determined by the deformation forces due to the centrifugal field being balanced by the interfacial tension. The first study on polymeric systems was performed by Patterson *et al.* (1971). They measured liquid polymers with viscosities up to 5000 P. Their maximum spinning speed was 6500 rpm. Elmendorp and de Vos (1986) built an instrument which allowed measurements on molten polymers. Temperatures up to 350 °C with an accuracy of 2 °C could be realized. Rotational speeds up to 25 000 rpm were possible. They also suggested that the time of measurement could be shortened by an extrapolation of the transient state and by a forced attainment of the equilibrium shape. This was achieved by spinning for a short while at a speed higher than the speed used at the final measurements. They loaded their samples by putting a thin slice of the less dense polymer between cylinders of the denser polymer. Problems with degassing and vibration were encountered. Elmendorp, de Wit, and Oudhaarlem (1988) described an improved spinning drop device with a maximum capacity of 300 °C and 20 000 rpm in which the problems of vibration and accessibility were reduced. However, the degree to which the vibration is suppressed by their 1-to-5 ratio gear drive and the problem of the outgassing are not discussed.

In addition to the interfacial tension, the development of the morphology of blends is crucially affected by the rheological properties of the blend components. The reason for this is that they determine the kinetics and mode of response of the system to the ever-changing stress

and velocity fields that are encountered in the complex processing machinery used for blend preparation (Elmendorp, 1985). For example, as a portion of the mixture enters a region of extensional flow the minor phase domains are stretched out into filaments which, in time, may break up into droplets. But if the filament enters a relatively quiescent region of flow before breakup has occurred, the elastic retraction of the filament can compete with breakup.

Some of the effects are quite subtle and are sensitive to parameters that are not easily measured by conventional means. For instance, it has been reported (Elmendorp, 1985; Gergen *et al.*, 1985) that the occurrence of a yield stress in the minor phase promotes the formation of a co-continuous, rather than a disperse, blend in extensional flow. Intuitively one might expect similar behavior for blends of liquid crystal polymers (LCPs) with isotropic polymers because most LCP melts have regions of shear-thinning yield stresses (see, for example, Chap. 13, "Rheology of Thermotropic Liquid Crystal Polymers" in Dealy and Wissbrun, 1990). However, the literature on the morphology of such blends is at least confusing, if not downright chaotic, in the diversity of observations indicative of great sensitivity of the response to system parameters. Of course, as pointed out for one such system (James *et al.*, 1990), there is also the important effect of interfacial tension to consider. It is reasonable to suppose that the interfacial tension of liquid crystal polymers may be anisotropic; that is, its value depends on the orientation of the LCP at the interface. The tensioextensometer offers the possibility of measuring anisotropic interfacial tension by measurements on specimens with orientation defined during sample preparation.

Development of the theory of the nonequilibrium spinning drop experiment for non-Newtonian fluids would permit inference of the combined effects of rheology and interfacial tension on droplet morphology of isolated drops. This offers an advantage over attempts to infer such effects from direct blending measurements because they are not confounded by the interfering effects of complex and time-dependent kinematics and of droplet interactions. Of course these complications are important in practice, but the data obtained from well-controlled observations would be invaluable for sorting out the effects. As discussed, melts or concentrated solutions with yield stresses are attractive candidates for such experiments, as are the LCP systems. Other interesting model systems are blends of monodisperse polymers of different molecular weights, which can be prepared so as to vary independently the melt viscosity and elasticity, and thereby permit assessment of their respective roles in determining blend morphology. Long-chain branch-

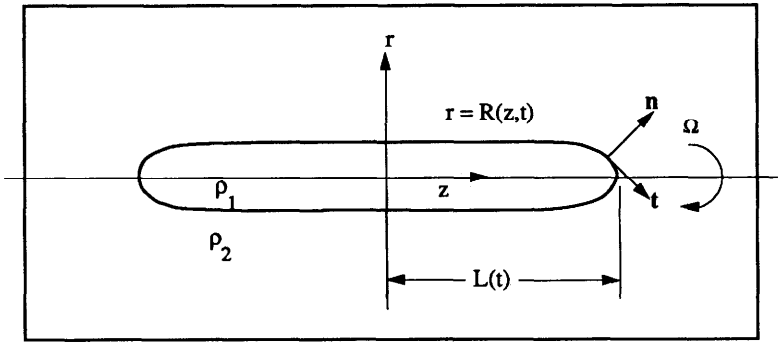


**FIG. 1.** Schematic of a long drop $L(t) \gg R(0,t) \overset{\text{def}}{=} R(t)$ of density $\rho_1 < \rho_2$ in a rapidly rotating container.

ing is another structural parameter worth studying because of its pronounced effect on viscoelasticity and upon elongational viscosities (Laun and Schuch, 1989).

## III. THE SPINNING DROP APPARATUS FOR MELTS

A spinning drop device is a rotating glass cylinder loaded with two immiscible liquids. The axis of the cylinder is rigorously perpendicular to gravity, and the constant speed of rotation is large enough for gravity effects to be negligible. The drop fluid is less dense and will centrifuge to the center of the container as in Fig. 1.

Rigid rotations of two immiscible liquids with gravity neglected are unconditionally stable when the light fluid is inside and the configuration of the interface minimizes a well defined potential (Vonnegut, 1942; Princen, Zia, and Mason 1967; Than *et al.* 1988; Joseph and Preziosi, 1987):

$$m = \int_0^L \left( \int_0^{2\pi} [T(R^2 + R_\theta^2 + R^2 R_x^2)^{1/2} - \tfrac{1}{8}[\![\rho]\!]\Omega^2 (R^2 - \overline{R}^2)^2] d\theta \right) dx, \tag{1}$$

where $R(\theta,x,t)$ is the radius of the drop, $\overline{R}$ is the root mean square radius, $L$ is the length of the drop, $T$ is the surface tension, $\Omega$ is the

angular velocity, and $[\![\rho]\!] = \rho_1 - \rho_2 < 0$ is the density difference of the fluid inside minus the fluid outside. The parameter

$$J = \frac{(\rho_2 - \rho_1)\Omega^2 \bar{R}^3}{T} \tag{2}$$

is very important. When $J > 4$ the spinning drop potential (1) can be minimized only by a cylinder of constant radius $R = \bar{R}$. Actually this solution can be realized only if there are end caps to restrain the expansion of the cylindrical like drop. If the drop is free to expand as $\Omega$ increases, it will elongate indefinitely when $J = 4$ in an extensional flow with $L$ increasing as $\bar{R}$ decreases. The drop will be a long cylinder of nearly constant diameter $D$ near to the maximum with rounded end caps. Calculations show that when $L/D \geqslant 4$ we can calculate the equilibrium surface tension for the case $J = 4$; i.e.,

$$T_{eq} = \frac{(\rho_2 - \rho_1)\Omega^2 D_{eq}^3}{32}, \tag{3}$$

where $D_{eq}(\Omega)$ is the maximum diameter of the equilibrium drop at the given value of $\Omega$ (Vonnegut, 1942).

A useful *relaxation function* which can be easily measured in experiments is the maximum diameter $D(t,\Omega)$ of the evolving drop at a fixed value of the angular velocity $\Omega$. The value $D_{eq}(\Omega)$ which determines the equilibrium value $T_{eq}$ of surface tension through Eq. (3) is the asymptotic value of the relaxation function

$$\lim_{t \to \infty} D(t,\Omega) \to D_{eq}(\Omega).$$

The two types of relaxation, I and II below, are of special interest.

A. Overly large initial diameter:

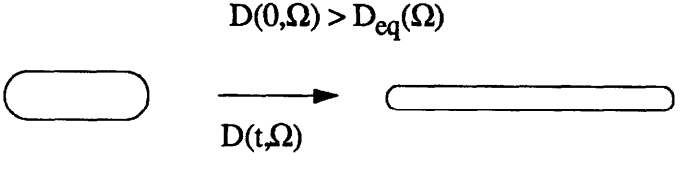

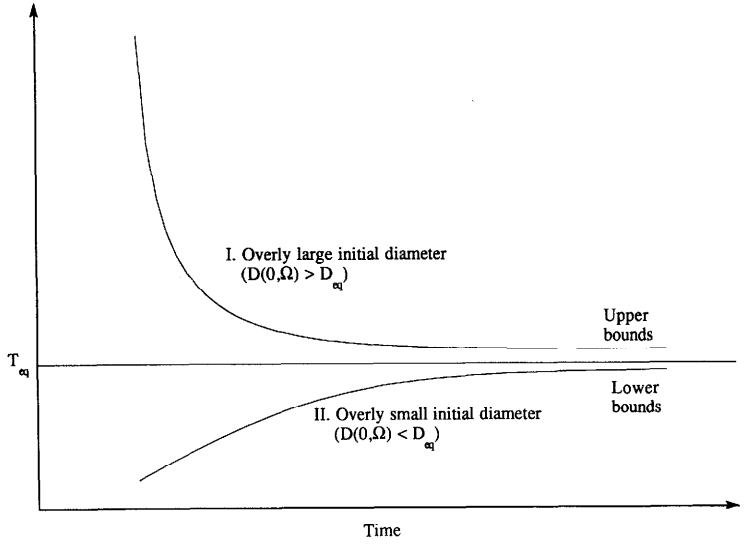


**FIG. 2.** Surface tension relaxation function and upper and lower bounds for $T_{eq}$.

B. Overly small initial diameter:

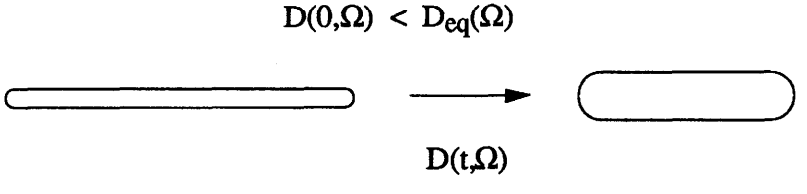


To get upper and lower bounds for the equilibrium interfacial tension, we define an interfacial tension relaxation function

$$T(t,\Omega) = \frac{(\rho_2 - \rho_1)\Omega^2 D^3(t,\Omega)}{32}. \tag{4}$$

The limiting value of this function as $t \to \infty$ is the equilibrium tension

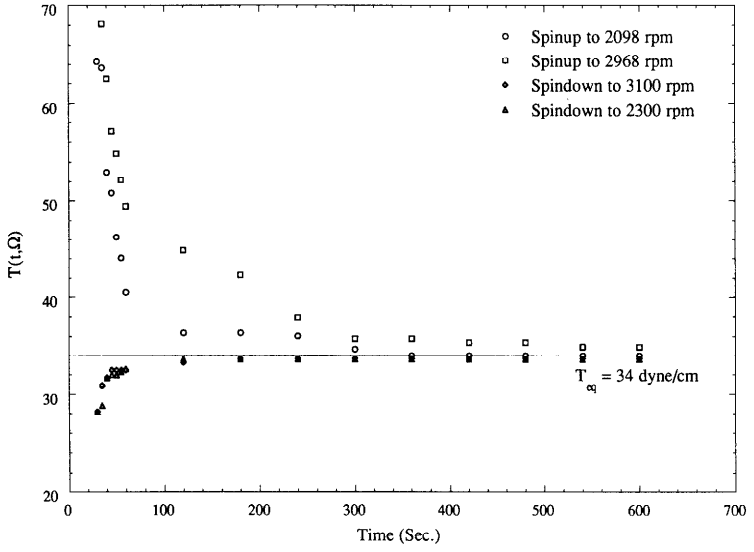


**FIG. 3.** Surface tension relaxation function for 20 cs poly(dimethyl-siloxane) in water. In this case, the asymptotic value of $T(t,\Omega)$ for large time was achieved. This value is the equilibrium tension $T_{eq} = 34$ dyn/cm.

$$T_{eq} = \lim_{t \to \infty} T(t,\Omega),$$

independent of $\Omega$ or $D(0,\Omega)$. All the relaxation functions I, for $D(0,\Omega) > D_{eq}(\Omega)$, lie above $T_{eq}$; all those in group II, $D(0,\Omega) < D_{eq}(\Omega)$, lie below $T_{eq}$.

Many different relaxation curves can be obtained, depending on $D(0,\Omega)$ and $\Omega$. They have a common asymptote, $T_{eq}$, as in Fig. 2. Some measured values of relaxation curves giving upper and lower bounds are exhibited in Fig. 3 and in other figures presented by Joseph, Arney, and Ma (1992).

We have developed an apparatus, called a tensioextensometer, for generating curves of relaxation for melted polymers like those shown in Fig. 3. A photograph of the instrument is shown in Fig. 4 and some details are drawn in Fig. 5 (Joseph and Hultman, 1991). The instrument permits placing polymers into a cylindrical tube, closing the ends, and providing means for driving the tube about its longitudinal axis while at the same time heating it to temperatures in the range of 300 °C.

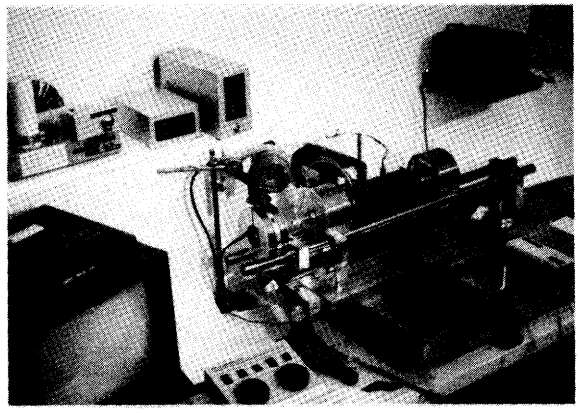

(a)

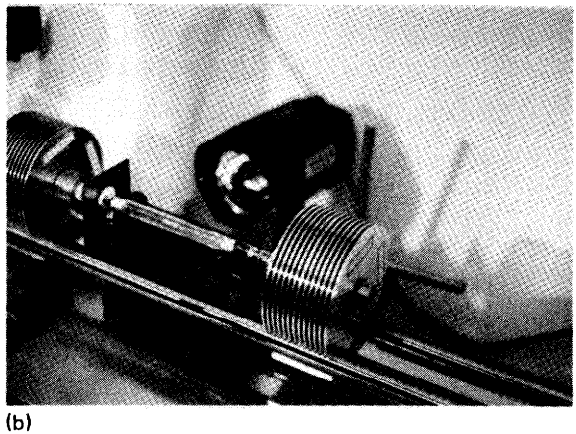

(b)

**FIG. 4.** Photographs of the tensioextensometer. (a) Overall view showing frame, cooling fins, oven, stroboscope, stages, camera, and monitor. (b) Cylinder assembly with top half of the oven removed [cf. Fig. 5(b)]. The inner diameter of the precision bore glass tube is 1.2 cm.

The tube is held very accurately about its center of rotation. Spring loaded end plungers in the tube provide for volume changes upon expansion or contraction of the polymers with changes in temperature. The instrument may be used to generate curves of volume expansion versus temperature. The springs are designed to provide enough pressure to prevent outgassing.

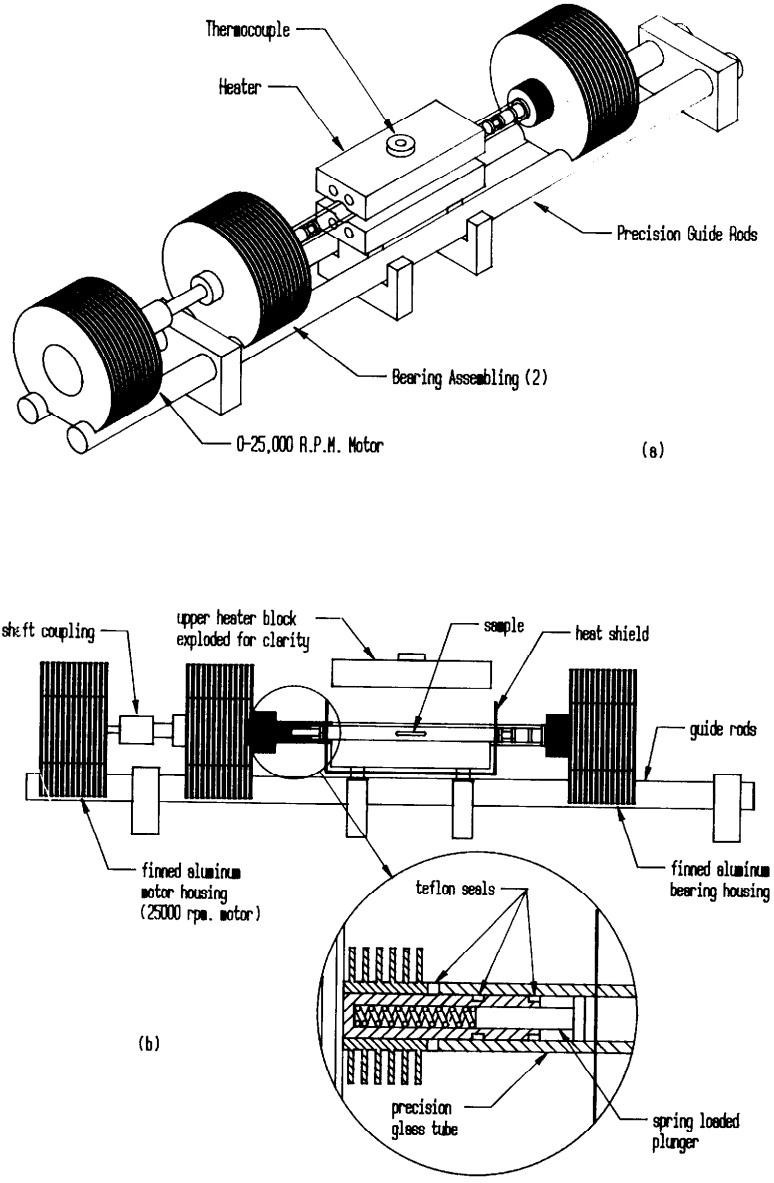


**FIG. 5.** Cartoon of tensioextensometer. (a) Overall view of the frame, oven, and cooling fins. (b) Details of cylinder assembly showing sample and how springs are used to maintain internal pressure to prevent outgassing.

A video camera of special design is used to monitor the drop. It is used in combination with a calibrated on-screen electronic reticule and a stroboscopic light to provide for real time diameter measurements.

The tensioextensometer follows prior art introduced by Patterson *et al.* (1971), Elmendorp and de Vos (1986), and Elmendorp, de Wit, and Oudhaarlem (1988) who also used a spinning drop apparatus with an oven. New features of this apparatus relate to the need to have high speeds (25 000 rpm) at high temperatures (300 °C) *without large vibrations.* These features are required for making precise transient measurements of the drop shape and radius which theory requires to back out rheological properties, extensional and yield stresses, as well as interfacial tension. Thermal isolation of bearings which communicate with an oven at 300 °C through metal shafts and supports is achieved in the present device by air cooling of the fin assemblies shown in Figs. 4 and 5. These fins allow us to keep the bearings at a low temperature indefinitely even when the furnace is at 300 °C. No special problems at elevated temperatures are encountered with our instrument. The suppression of large vibrations at high speeds is very much a question of balanced delivery of torques and rigidity of construction. Our earlier design which used pulleys could not be made to suppress vibration, even with the rigid track construction of two-sided supports in evidence in figures. We were successful in suppressing vibrations by using a direct and balanced drive coupling to the shaft and precision bearings. The two-sided support of the cylinder assembly allows us to easily load samples and to apply spring pressure to the sample ends. The springs shown in Fig. 5 have a dual purpose. First, they give under pressure, allowing the sample to expand under heating. At the same time they maintain enough pressure to completely suppress the outgassing which occurs, for example, when the polymer's plasticizers or residual monomers vaporize, or when other dissolved gases (e.g., air) are released by the molten polymer. A result of conscious control of pressure by spring end loads is a perfect interface uncontaminated by air in every instance. By monitoring the displacement of the spring after heating the sample we can compute the volume change upon heating of a sample of known mass. This means that the tensioextensometer can be used to construct graphs of density versus temperature, as well as to measure rheological properties and interfacial tension.

Our tensioextensometer will not work if the matrix material is not transparent. It will not work if the two materials have exactly the same density. If they do have the same density at one temperature, they will have different densities at another temperature. Since the tension is

proportional to the product of the square of the angular velocity times the density difference, we can accommodate a small difference by spinning fast. We have actually generated temperature versus tension graphs for heavy crude in water in the region where the ratio of the densities passes through one.

## IV. EXPERIMENTAL

For initial studies low density polyethylene (LDPE), polystyrene (PS), and polymethylmethacrylate (PMMA) were selected since interfacial tension data for pairs of these polymers are published (Wu, 1969; Elmendorp and de Vos, 1986). The stock polymers were purchased commercially (from Cadillac Plastics, Troy, MI and Almac Plastics, New York, NY) in the form of long rods with a 1/2 in. diameter. Their zero shear viscosities were measured with a Rheometrics RMS 800 rheometer using the parallel plate fixtures. Their densities, molecular weights, and zero shear viscosities are given in Table I.

To make the matrix, or outer phase, two short rods of the heavier polymer were cut from the stock, their diameters were slightly reduced so that they fit snugly inside the glass tube, and their ends were accurately squared. Into one of the pieces, a small, cylindrical hole with a square bottom was drilled, with a diameter chosen to be slightly larger than the estimated equilibrium diameter and a depth that is 6–8 times the diameter. A special drill bit with a square tip was used to make the hole a perfect square cylinder. The drop phase consisted of a short cylinder of the lighter polymer with a diameter that was slightly smaller than the hole drilled in the matrix rod. The two matrix rods and the drop cylinder were cleaned in an ultrasonic bath of methanol and then in a bath of hydrochloric acid and then rinsed and dried. The drop cylinder was inserted into the matrix hole and any excess was trimmed with a razor blade. Then, the two matrix pieces were inserted into the glass tube, so that the hole was covered up. Then, the glass tube was mounted on the tensioextensometer and spun up to a moderate rpm, after which the oven was turned on and set to the desired temperature. Upon melting, the two matrix pieces fused together and the drop formed a cylindrical shape with rounded end caps, as shown in Fig. 1.

Originally, a vacuum was applied to the polymer glass tube assembly during heating to remove from the sample any entrapped air or volatile components, such as plasticizers or residual monomers. Further experiments showed that this degassing was unnecessary with the improved machining of the polymers to perfect fit and the new spring loading

which maintained an adequate pressure in the molten polymers. No air bubbles are observed during the experiments. The drop diameter and length was measured at regular intervals.

## V. RELAXATION CURVES

Relaxation curves are useful only when the relaxation is slow enough to measure and when the relaxation is monotone. This is the usual situation for highly viscous fluids, especially when the heavy fluid which is centrifuged to the cylinder wall is very viscous, as in the case of polymer melts. For these systems the rheometrical properties of the relaxation can be even more important than the equilibrium values of surface tension. In general, relaxation curves depend strongly on the rotation speed, the volume fraction, the container dimensions, the bulk properties of the two liquids, the viscosities, densities, and relaxation times for each liquid, as well as on interfacial properties. The set of all these parameters, as well as the initial conditions, determine the *relaxation properties of a system* of two liquids in a container. We italicized the main idea in the last sentence to draw attention to the difference between relaxation of a *system* and the relaxation of a fluid. Usually we think of viscoelastic fluids as having some mean time of relaxation. We may define a mean time of relaxation for a system even when the two fluids are Newtonian. Roughly speaking, this time is the time taken for the *system* to relax into rigid rotation after a perturbation. The idea makes sense only when rigid rotation is stable; then the time of relaxation for the system can be regarded as the decay rate for a stable perturbation. In the case of Newtonian fluids, this stability can be guaranteed unconditionally [see Joseph and Preziosi (1987)]. Suppose that $\hat{\mathbf{u}}$ is the velocity perturbing rigid rotation $\mathbf{e}_\theta \Omega r$. Then it can be shown that

$$\frac{d\mathscr{E}}{dt} + \frac{dm}{dt} = -\mathscr{D}[\hat{\mathbf{u}}], \tag{5}$$

where

$$\mathscr{E} = \int_{V_1} \rho_1 |\hat{\mathbf{u}}|^2 \, dv_1 + \int_{V_2} \rho_2 |\hat{\mathbf{u}}|^2 \, dv_2$$

is the disturbance energy in the region $V_1$ and $V_2$ occupied by the two liquids, $m$ is the interfacial potential (1), and

$$\mathscr{D}[\hat{\mathbf{u}}] = \int_{V_1} \mu_1 \mathbf{D}^2[\hat{\mathbf{u}}]\, dv_1 + \int_{V_2} \mu_2 \mathbf{D}^2[\hat{\mathbf{u}}]\, dv_2$$

is the disturbance dissipation (and $\mathbf{D}[\hat{\mathbf{u}}]$ is the rate of strain). The analysis of the evolution equation (15) by Joseph and Preziosi shows that $\mathscr{E}$ and $\mathscr{D}$ decay to zero and $m$ tends to a minimum value over functions $R(\theta,z)$ in a function space in the sense of the calculus of variations. This is why the parameter $J$ defined in Eq. (2) becomes important. We could linearize Eq. (5) for small perturbations of rigid motion and the equilibrium drop, using normal modes

$$\hat{\mathbf{u}} = e^{\sigma t} e^{in\theta} \tilde{\mathbf{u}}(r,z),$$

$$R - \overline{R} = e^{\sigma t} e^{in\theta} R(z), \tag{6}$$

where $\sigma$, the growth rate, appears as the eigenvalue of the reduced system. In fact, there is a linearized version of Eq. (5) which is in the form

$$\sigma(\tilde{\mathscr{E}} + \tilde{m}) = -\tilde{\mathscr{D}}, \tag{7}$$

defining $\sigma$ as an eigenvalue depending on all the system parameters. Actually we know from the analysis of Joseph and Preziosi that $\sigma$ is real and negative for all eigenvalues. The eigenvalues give the rate of decay of small disturbances of the equilibrium of the system and the slowest rate of decay, *the smallest* $|\sigma|$, *can be said to define a relaxation time* $\tau_s = \min|\sigma|$ *for the system*. We want to calculate this eigenvalue, to see how it depends on system parameters, in this case and in the case of viscoelastic fluids. It will be possible to obtain some properties of $\tau_s$ through careful scaling of the equations governing the linear theory of stability of the rotating equilibrium drop, but this problem cannot be fully resolved without numerical analysis.

The determination of relaxation times for a system of two viscoelastic liquids is more complicated than in the Newtonian case. Even the problem of stability of the state of rest of viscoelastic fluid gives rise to complex rather than real eigenvalues. This study can be carried out with generality using the Boltzmann constitutive equation for linear viscoelasticity. The same constitutive equation is known to give a correct description of any incompressible viscoelastic fluid with instantaneous elasticity in all sufficiently small motions perturbing rigid motion. We are interested in carrying out a mathematical analysis of the linearized problem of stability of rigid motions of one fluid in a cylindrical container. The problem can be reduced to a coupled pair of partial differ-

ential equations of order four for two components of velocity. This problem is very nonlinear in the eigenvalue $\sigma$ for disturbances proportional to $\exp(\sigma t)$. The eigenvalue $\sigma$ enters into this problem linearly in the usual way and nonlinearly through the "complex viscosity"

$$\eta^*(\sigma) = \int_0^\infty G(s)e^{-\sigma s}\,ds, \tag{8}$$

where $G(s)$ is the Boltzmann relaxation kernel. This simplifies to a rational function

$$\eta^*(\sigma) = \frac{\eta}{\lambda\sigma + 1} \tag{9}$$

for Maxwell models $G(s) = (\eta/\lambda)\exp(-s/\lambda)$ with a single time $\lambda$ of relaxation ($\eta$ is the viscosity).

We carried out an analysis of the stability of the state of rest in a cylindrical container of radius $a$ for periodic disturbances proportional to $e^{iax}$, where $x$ is along the axis and the end caps have been removed to infinity. The analysis follows along the lines laid down on pages 216–219 of Joseph (1976) where it leads to a dimensionless dispersion there labeled (94.60), which can be expressed here as

$$2E\sigma = -1 \pm \sqrt{1 - 4E(\alpha^2 + \Lambda_1^2)}, \tag{10}$$

where $\Lambda_1 = 3.83$ is the smallest eigenvalue in a discrete set determined by roots of the Bessel function $J_1(\Lambda_n) = 0$ and

$$E = \lambda\eta/\alpha^2\rho \tag{11}$$

is the elasticity number. If $E \neq 0$ and $4E(\alpha^2 + \Lambda_1^2) > 1$, then disturbances must oscillate with a frequency

$$\omega = \frac{1}{2E}\sqrt{1 - 4E(\alpha^2 + \Lambda_1^2)}$$

as they decay. Short waves with large $\alpha$ will oscillate. All waves oscillate as they decay if the fluid is sufficiently elastic; that is, if

$$E > 1/4\Lambda_1^2 = 0.017. \tag{12}$$

This shows that the intuitively appealing idea that the relaxation time for a system of two highly viscous polymers in the spinning drop rheometer is determined in a Newtonian approximation because they move so slowly cannot be correct in a strict sense.

Let us suppose that we have a long equilibrium drop, a cylinder of radius $R$ with rounded end caps, with $J$ ever so slightly less than 4. We know that in the final stage of relaxation, say $t \geqslant t_0$, the approach to equilibrium is exponential and the longest lasting disturbance proportional to $e^{-mt}$. Hence we may suppose that in the final stage of decay

$$R(t) - R_\infty = (R_0 - R_\infty)e^{-m(t-t_0)}. \tag{13}$$

Equation (13) says that the final stage of relaxation is exponential, so that we may fit an exponential to the data [measure values of $R(t)$] to determine $R_\infty$ and $m$. Next we consider the application of Eq. (13) to experiments.

## VI. APPLICATIONS OF CURVE FITTING TECHNIQUE TO EXPERIMENTAL DATA

Some results were given in detail by Verdier (1990) who used the method of Patterson *et al.* (1971) to analyze his data. This method is based on the observation that after a relatively short induction period

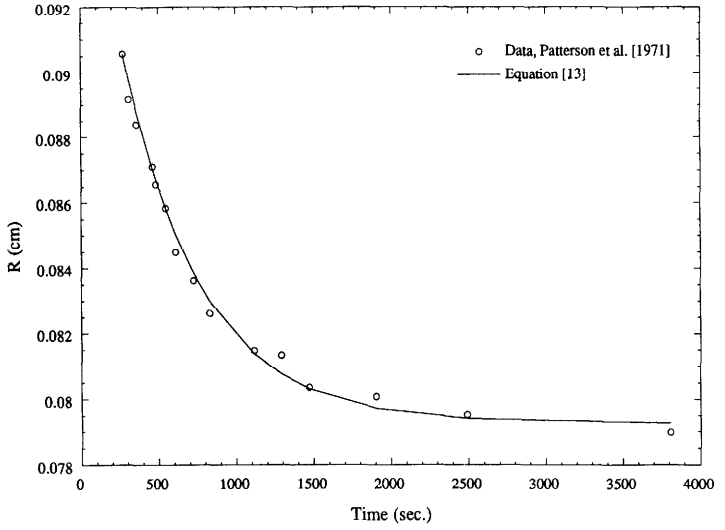


**FIG. 6.** Data from Patterson *et al.* (1971), Fig. 4 fitted to Eq. (13) with $R_\infty = 0.079$ cm and $m = 0.084$ min$^{-1}$. This value of $R_\infty$ gives a $T = 3.6$ dyn/cm, which is close to the reported value of 3.4 dyn/cm.

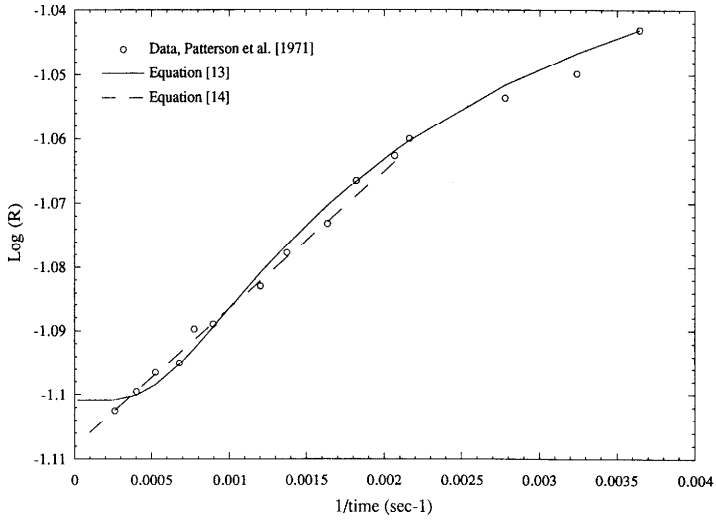


**FIG. 7.** Data from Patterson *et al.* fitted to Eq. (13) (solid line), and Eq. (14) (dotted line) plotted as $\log(R)$ vs $1/t$. Notice the divergence at small 1/time.

there was a linear relationship between the logarithm of the drop length and the reciprocal of time. By extrapolating this way, Patterson *et al.* could reduce the time of measurements from hours to 10–20 min.

Patterson, Hu, and Grindstaff (1971) measured the length of a deforming drop. They say that "...Examination of the change of bubble length with time revealed that after a relatively short induction period there was a linear relationship between the logarithm of the bubble length and the reciprocal of the time...Extrapolation of the straight-line portion of the results to infinite time provided a measure of the steady state interfacial tension." By extrapolating this way, Patterson *et al.* (1971) reduced the measurement of steady state values from over 3 h to 10–20 min. Verdier (1990) plotted the logarithm of the drop diameter for several polymer melts against the reciprocal of the time and also found a straight line which could be extrapolated to infinite time. Obviously this extrapolation can be viewed as a manifestation of the final approach to equilibrium.

Patterson *et al.* did not give any theoretical motivation for their method of plotting and their interpretation of the extrapolation is actually against theory as the following argument shows. Let $L_\infty$ be the equilibrium length of the drop. They find a linear region where

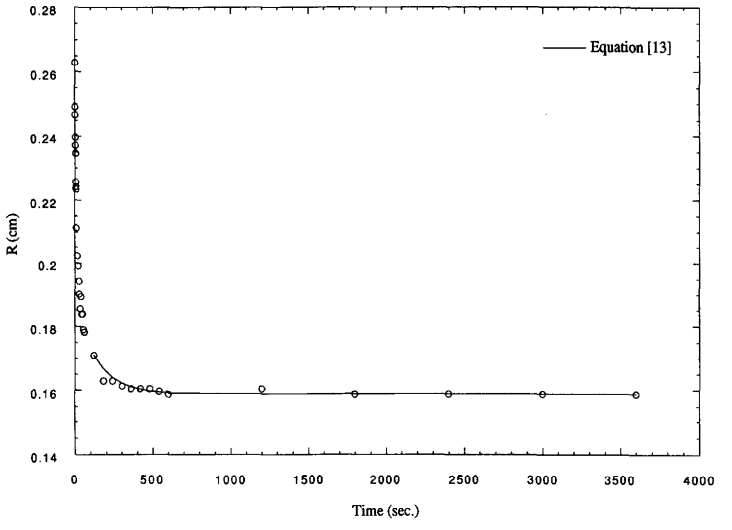


**FIG. 8.** 100 000 cs PDMS in glycerol with the angular speed $\Omega$ increased to 3208 rpm. $R_\infty = 0.159$ cm ($T = 32.4$ dyn/cm), $m = 0.428$ min$^{-1}$.

$$\log L_\infty - \log L(t) = \frac{c}{t}$$

for some constant $c$. Then

$$\frac{L_\infty}{L(t)} = e^{c/t},$$

$$L(t) = L_\infty e^{-c/t}. \tag{14}$$

However, the approach of a small disturbance of an equilibrium, which is independent of time, must necessarily be exponential with decay like $e^{-mt}$ and not like $e^{-c/t}$.

The idea of using the approach to equilibrium to shorten the time of measurement is a good one and can be implemented using a correct theory. This approach yields a measured system time of relaxation $m$ as well as the interfacial tension $T$. Suppose that $R$ is precisely measured at two times $t_1 > t_0$, $t_2 > t_1$. Then we may eliminate $m$ in (13) and find that $R_\infty$ is determined by

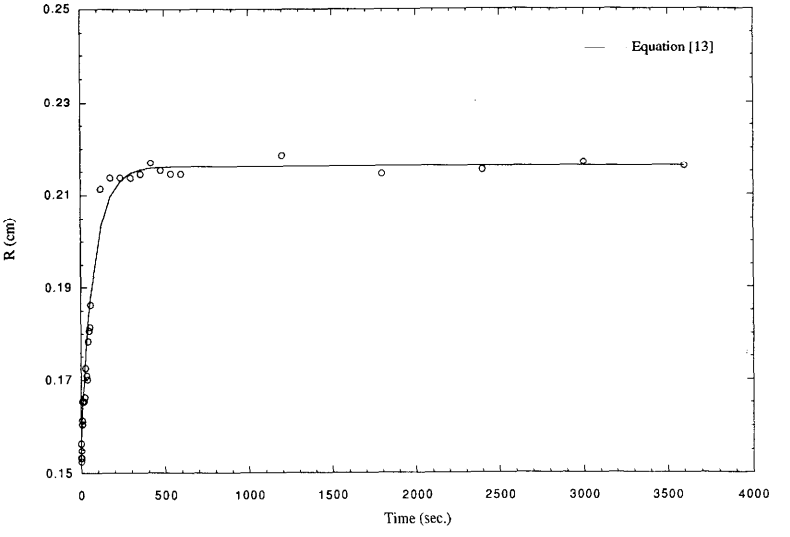


**FIG. 9.** 100 000 cs PDMS in glycerol with the angular speed $\Omega$ decreased to 2032 rpm. $R_\infty = 0.216$ cm ($T = 32.7$ dyn/cm) and $m = 0.75$ min$^{-1}$.

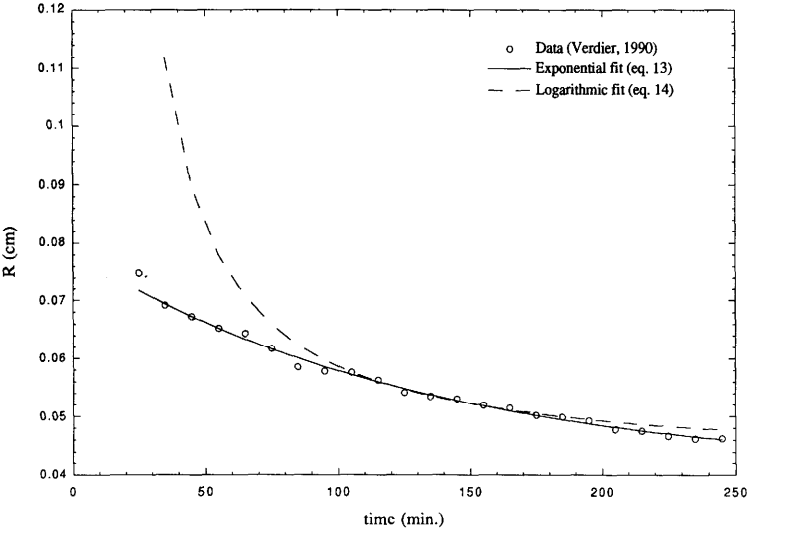


**FIG. 10.** Data from Verdier (1990). LDPE in PMMA at a temperature of 200 °C with the angular speed $\Omega$ increased to 12 000 rpm. $R_\infty = 0.0405$ cm ($T = 8.72$ dyn/cm), $m = 7.8 \times 10^{-3}$ min$^{-1}$.

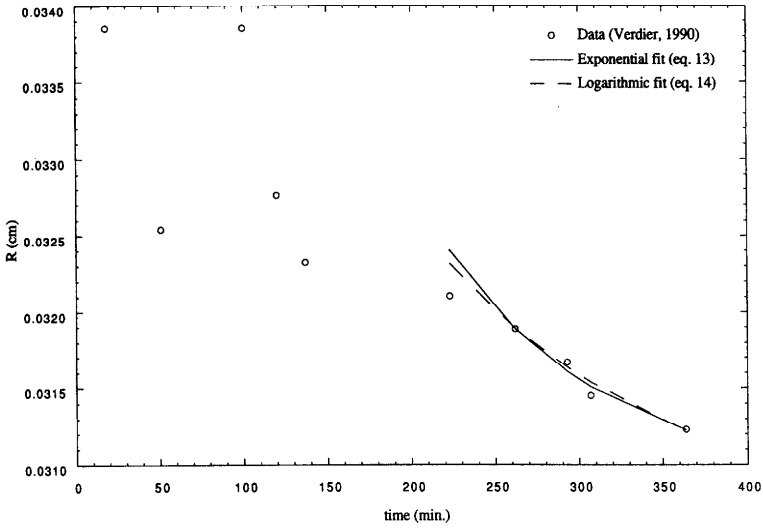


**FIG. 11.** Data from Verdier (1990). PS in PMMA at a temperature of 200 °C with the angular speed $\Omega$ increased to 15 046 rpm. $R_\infty = 0.0309$ cm ($T = 2.09$ dyn/cm), $m = 11.0 \times 10^{-3}$ min$^{-1}$.

$$\left[\frac{R(t_0) - R_\infty}{R(t_1) - R_\infty}\right]^{t_2 - t_1} = \left[\frac{R(t_1) - R_\infty}{R(t_2) - R_\infty}\right]^{t_1 - t_0}. \tag{15}$$

Returning then to (13) with $R_\infty$, we get $m$. Since the data are inevitably scattered, we may choose optimum values of $R_\infty$ and $m$ to fit data $R(t_i)$ using (13) for all points $(t_i, R_i)$ by minimizing the error function

$$E(R_\infty, m) = \sum_{i=1}^{N} [R_i - R(t_i)]^2. \tag{16}$$

We used Powell's algorithm (Press *et al.*, 1986) to perform the minimization of (16). This method appears to work well in all the cases tried by us.

Figure 4 of Patterson *et al.* shows the $\log(L)$ vs 1/time for polyisobutylene (PIB, 70 000 cp) in polydimethylsiloxane (PDMS, 103 000 cp). We carefully estimated the values of the points and converted the drop lengths to diameters based on the assumptions that the drop volume was exactly 0.03 ml and that the drop's length to diameter ratio is

large enough so that $V = \pi R^2 L$. We then fitted this data to Eq. (13) and the results are displayed in Fig. 6. Then, to compare results, a plot of $\log(R)$ vs 1/time for both the data and the fitted exponential curve are shown in Fig. 7. We call attention to the fact that Patterson's straight line in the plot is nearly identical to our fitted exponential when $1/t$ is not small, but they diverge for small values of $1/t$.

We measured drop diameter as a function of time for 100 000 cs polydimethyl siloxane (Dow-Corning 200 Fluid), a polymer melt with a reliable viscosity, in glycerol when the angular velocity is increased (Fig. 8) and decreased (Fig. 9). These measurements were done with the spinning drop tensiometer described in Than *et al.* (1988) and using a video camera and recorder with an on-screen clock and calibrated reticles. In both cases, the data is easily fitted to Eq. (13) so it apparently works well in both the spin-up and spin-down cases. It is interesting to point out that the relaxation times are different for the spin-up ($m = 0.428$ min$^{-1}$) and spin-down ($m = 0.75$ min$^{-1}$) experiments; we do not know the reason for this difference. Figures 10, 11, and 12 are taken from Verdier (1990) and give results for three different polymer pairs. We fitted Eq. (13) to a number of different fluid systems, and values for surface tension and relaxation time ($m$) are displayed in Table II. The plots that accompany these values can be found in Arney (1992).

The comparison (Figs. 6–11) of the method of fitting introduced by Patterson *et al.* [Eq. (14)] with the theoretically based method of exponential fitting [Eq. (13)] rise to near agreement for a limited range of data. The extrapolation to the equilibrium radius is different, but not greatly different, for the two methods. The method of exponential fitting works well in all cases and allows one to make extrapolations of data taken from earlier times than the method of Patterson *et al.* We estimate that the method of exponential fitting can shorten the time of measurement over and above the shortening already achieved by Patterson *et al.*

## VII. EXTENSIONAL FLOW

The idea of a tension relaxation function which we have introduced in our discussion of lower and upper bounds needs further study from a theoretical point of view. A theoretical analysis appropriate to the situation following spin-up or spin-down is constructed as follows. We first suppose that we have changed the angular velocity from one constant value to another constant value $\Omega$ at some time past. After a short time

**TABLE II.** Table of results.

| Inside material | Outside material | Ω (rpm) | Temp (°C) | Interfacial tension (dyn/cm) | $m$ ($\text{min}^{-1}$) |
|---|---|---|---|---|---|
| PIB (70 000 cp)[a] | PDMS (103 000 cp) | | | 3.6 | 0.084 |
| 100 000 cs PDMS | Glycerol | 3208 | 25 | 32.4 | 0.428 |
| 10 000 cs PDMS | Glycerol | 2320 | 25 | 26.0 | 0.225 |
| LDPE[b] | PMMA | 12 000 | 250 | 12.0 | 0.020 |
| LDPE[b] | PMMA | 12 000 | 200 | 8.72 | 0.0078 |
| LDPE[b] | PMMA | 12 000 | 225 | 14.6 | 0.0069 |
| LDPE[b] | PMMA | 12 000 | 250 | 5.38 | 0.0073 |
| PS[b] | PMMA | 15 046 | 200 | 2.09 | 0.011 |
| PS[b] | PMMA | 15 046 | 225 | 1.33 | 0.0085 |
| PS[b] | PMMA | 15 046 | 250 | 0.25 | 0.0116 |
| LDPE[b] | PS | 15 046 | 225 | 4.32 | 0.0121 |
| LDPE[b] | PS | 15 046 | 250 | 5.61 | 0.0228 |

[a]Data from Patterson *et al.* (1971).
[b]Data from Verdier (1990).

spin-up or -down is achieved in both fluids which then rotate rigidly with the container so that

$$u_\theta = \Omega r. \tag{17}$$

It is further assumed that the drop dimensions continue to change for a long time even after the spin-up represented by Eq. (17) has been achieved. Eventually the drop reaches its equilibrium size and shape consistent with Eq. (1). The seminal proposition, introduced by Hsu and Flumerfelt (1975), is that the adjustment to equilibrium takes place as an unsteady pure cylindrical extension with a velocity field given by

$$u_r = -\tfrac{1}{2}\dot{s}(t)r, \quad u_z = \dot{s}(t)z, \tag{18}$$

where $\dot{s}(t)$ is the rate of extension and

$$\dot{s}(t) \to 0 \tag{19}$$

at $t \to \infty$. Obviously, this proposition must fail at the walls of the container, so that our assumption is a local approximation in the region neighboring the drop. We find that when the effects of the container walls are neglected, the solution corresponding to rigidly rotating extensional flow (17), (18), and (19) satisfies all the governing equations for a long drop satisfying condition (18) except for an imbalanced shear stress on the rounded end caps of the drop. In fact, the shear stress is

balanced on all flat portions of the long cylinder and at the tips $r = 0$, $z = \pm L$ of the end caps. If the drop is relatively viscous we might except a weak secondary motion to develop in the end cap, which is definitely neglected and may be negligible. The only approximation for our analysis is that the shape of the drop, but not its dimensions, is given by the equilibrium shape even while the drop is expanding or contracting. This assumption is a link between the dynamics of cylindrical extension and the equilibrium configuration of the two rotating fluids and it allows us to generalize and close the Hsu–Flumerfelt theory. The final result is a nonlinear ordinary differential equation for the radius $R(t)$ of a long drop whose solutions appear to be consistent with observations in a limited region of parameters and, in particular, agree with acceptable accuracy with data already published by Hsu and Flumerfelt (1975). All these assumptions, pure unsteady extension, neglect of the effects of container walls, the unbalanced shear stress, and the retention of equilibrium shape of the drop under nonequilibrium conditions, can and will be tested by direct numerical simulations.

The rate of strain $\mathbf{D}[\mathbf{u}]$ for the rotating extensional flow (18) and (19) is given by

$$\mathbf{A}_1 = 2\mathbf{D}[\mathbf{u}] = \mathbf{L} + \mathbf{L}^T, \tag{20}$$

where the components of $\mathbf{L} = \nabla\mathbf{u}$ in cylindrical coordinates $r,\theta,z$ are given by

$$[\mathbf{L}] = \begin{bmatrix} \dfrac{\partial u_r}{\partial r} & -\dfrac{u_\theta}{r} & 0 \\ \dfrac{u_\theta}{r} & \dfrac{u_r}{r} & 0 \\ 0 & 0 & \dfrac{\partial u_z}{\partial z} \end{bmatrix} = \begin{bmatrix} -\dot{s}/2 & -\Omega & 0 \\ \Omega & -\dot{s}/2 & 0 \\ 0 & 0 & \dot{s} \end{bmatrix}. \tag{21}$$

The stress in an incompressible simple fluid may be written as

$$\mathbf{T} = -p\mathbf{1} + \mathbf{S} \tag{22}$$

where $p$ is the "reaction pressure" and is not given as a constitutive equation and $\mathbf{S}$ is the extra stress which is related to deformation, *a priori*, by constitutive assumptions. In simple fluids [see, for example, Joseph (1990), Appendix C]

$$S = \overset{t}{\underset{\tau = -\infty}{\boldsymbol{F}}} [\mathbf{C}_t(\tau) - \mathbf{1}], \tag{23}$$

is given by an isotropic tensor valued functional of the Cauchy–Green tensor

$$\mathbf{C}_t(\tau) = [\nabla \chi_t(\mathbf{x},\tau)]^T [\nabla \chi_t(\mathbf{x},\tau)], \tag{24}$$

such that the stress of any rigid motion $\mathbf{C}_t(\tau) = \mathbf{1}$ vanishes, $F(\mathbf{0}) = \mathbf{0}$.

The power series expansion of

$$\mathbf{C}_t(\tau) - \mathbf{1} = \sum_{n=1}^{\infty} \frac{(\tau - t)^n}{n!} \mathbf{A}_n(t) \tag{25}$$

introduces the Rivlin–Ericksen tensors $\mathbf{A}_n$, related to $\mathbf{A}_1$ through a recursion relation of the form

$$\mathbf{A}_{n+1} = \frac{\partial \mathbf{A}_n}{\partial t} + (\mathbf{u}\cdot\nabla)\mathbf{A}_n + \mathbf{A}_n\mathbf{L} + \mathbf{L}^T\mathbf{A}_n. \tag{26}$$

For extensional flow $\mathbf{L}$ and $\mathbf{A}_1$ are independent of $\mathbf{x}$ and

$$\mathbf{L} = \tfrac{1}{2}\mathbf{A}_1 + \boldsymbol{\omega}, \tag{27}$$

where $\boldsymbol{\omega}^T = -\boldsymbol{\omega}$ is skew symmetric. From Eqs. (26) and (27) we compute

$$\mathbf{A}_2 = \frac{\partial \mathbf{A}_1}{\partial t} + \mathbf{A}_1^2 \tag{28}$$

then

$$\mathbf{A}_3 = \frac{\partial^2 \mathbf{A}_1}{\partial t^2} + 3\mathbf{A}_1 \frac{\partial \mathbf{A}_1}{\partial t} + \mathbf{A}_1^3, \tag{29}$$

and so on. Hence

$$\mathbf{C}_t(\tau) = \exp\left( - \int_\tau^t \mathbf{A}_1(\tau')d\tau' \right). \tag{30}$$

It follows from Eq. (30) that the extra stress in rotating unsteady extensional flow is independent of place and depends only on time. Since $F$ is an isotropic functional it is diagonal when $\mathbf{C}_t(\tau)$ is diagonal, as in the case of unsteady pure cylindrical extension (18), and

$$\begin{bmatrix} S_{rr} & S_{r\theta} & S_{rz} \\ S_{r\theta} & S_{\theta\theta} & S_{\theta z} \\ S_{rz} & S_{\theta z} & S_{zz} \end{bmatrix} = \begin{bmatrix} \sigma(t) & 0 & 0 \\ 0 & \psi(t) & 0 \\ 0 & 0 & \zeta(t) \end{bmatrix}. \tag{31}$$

Different and special forms for $\sigma$, $\psi$, and $\zeta$ are implied by different constitutive models. We shall return to this briefly later.

## VIII. EVOLUTION EQUATION FOR THE RADIUS OF THE DROP

We may write the $r$ and $z$ components of the equations of motion, using Eqs. (17), (18), and (31) as

$$\rho\left(\frac{\partial u_r}{\partial t} - \Omega^2 r\right) = \frac{\partial}{\partial r}\left(-p + \sigma - \frac{\rho}{2}u_r^2\right) \tag{32}$$

and

$$\rho\frac{\partial u_z}{\partial t} = \frac{\partial}{\partial z}\left(-p + \zeta - \frac{\rho}{2}u_z^2\right). \tag{33}$$

These last two equations may also be written as

$$\frac{\partial}{\partial r}\left(-p + \sigma - \frac{\rho}{2}u_r^2 + \frac{\rho}{4}\ddot{s}r^2 + \frac{\rho\Omega^2 r^2}{2}\right) = 0 \tag{34}$$

and

$$\frac{\partial}{\partial z}\left(-p + \zeta - \frac{\rho}{2}u_z^2 - \frac{\rho}{2}\ddot{s}z^2\right) = 0. \tag{35}$$

After integrating Eqs. (34) and (35) we find that

$$-p + \sigma(t) + \zeta(t) - \frac{\rho}{2}(\dot{s}^2 + \ddot{s})z^2 - \frac{\rho}{2}\left(\frac{\dot{s}^2}{4} - \frac{\ddot{s}}{2} - \Omega^2\right)r^2 + f(t) = 0, \tag{36}$$

where $f(t)$ is an arbitrary function of time which may be eliminated using the normal stress balance at the end tip $r = 0$, $z = L$ (see Fig. 1) where $\mathbf{n} = \mathbf{e}_z$ and

$$[\![-p + \zeta]\!] + 2H_L T = 0, \tag{37}$$

where $2H_L$ is the total curvature at $r = 0$, $z = L$ and

$$[\![\cdot]\!] = (\cdot)_1 - (\cdot)_2. \tag{38}$$

After combining Eqs. (36) and (37) we find that

$$[\![f(t)]\!] = \frac{[\![\rho]\!]}{2}(\dot{s}^2 + \ddot{s})L^2 - [\![\sigma(t)]\!] + 2H_L T. \tag{39}$$

This allows us to replace the unknown $[\![f(t)]\!]$ with the unknown $H_L$. After forming the jump relation across $R(z,t)$, using Eqs. (36) and (39), we get

$$-[\![p]\!] + [\![\zeta(t)]\!] + \frac{[\![\rho]\!]}{2}(\dot{s}^2 + \ddot{s})(L^2 - z^2)$$

$$= \frac{[\![\rho]\!]}{2}\left(\frac{\dot{s}^2}{4} - \frac{\ddot{s}}{2} - \Omega^2\right)R^2 - 2H_L T. \tag{40}$$

It is necessary to verify that the solution $(u_r, u_\theta, u_z, p)$, which we have proposed satisfies the interface conditions for the stress. Let $\mathbf{n}$ be the outward normal to the drop and $\mathbf{t}$ the unit tangent to the curve $R(z,t)$. Then

$$\mathbf{n} = \cos\alpha \mathbf{e}_r - \sin\alpha \mathbf{e}_z,$$

$$\mathbf{t} = \sin\alpha \mathbf{e}_r + \cos\alpha \mathbf{e}_z, \tag{41}$$

$$\mathbf{Tn} = -p\mathbf{n} + \sigma \mathbf{e}_r \cos\alpha - \zeta \mathbf{e}_z \sin\alpha, \tag{42}$$

$$[\![\mathbf{e}_\theta \cdot \mathbf{Tn}]\!] = 0, \tag{43}$$

$$[\![\mathbf{t} \cdot \mathbf{Tn}]\!] = \sin\alpha \cos\alpha [\![\sigma - \zeta]\!], \tag{44}$$

and

$$[\![\mathbf{n} \cdot \mathbf{Tn}]\!] = [\![-p]\!] + [\![\sigma]\!]\cos^2\alpha + [\![\zeta]\!]\sin^2\alpha. \tag{45}$$

The shear stress (43) is satisfied automatically but $[\![\mathbf{t} \cdot \mathbf{Tn}]\!]$ cannot vanish unless $\sin\alpha \cos\alpha = 0$, at the equator $z = 0$, $\sin\alpha = 0$ or at the tip of the end cap $r = 0$, $\cos\alpha = 0$.

In the case of a long drop, a cylinder with rounded end cap, like the one shown in Fig. 1, $\sin\alpha$ is near to zero all along the cylinder and

$$[\![\mathbf{n} \cdot \mathbf{Tn}]\!] = -[\![p]\!] + [\![\sigma]\!] = -\frac{T}{R}. \tag{46}$$

In this case, which can be achieved for large values of $\Omega$, we get $[\![\mathbf{t}\cdot\mathbf{Tn}]\!]\approx 0$ everywhere but at the end caps where $\sin\alpha\cos\alpha\neq 0$. The pressure in Eq. (46) may be eliminated using Eq. (40):

$$-\frac{T}{R}+[\![\zeta-\sigma]\!]+\frac{[\![\rho]\!]}{2}(\dot{s}^2+\ddot{s})(L^2-z^2)$$

$$=\frac{[\![\rho]\!]}{2}\left(\frac{\dot{s}^2}{4}-\frac{\ddot{s}}{2}-\Omega^2\right)R^2-2H_LT. \tag{47}$$

This equation was obtained by Hsu and Flumerfelt (1975) except that inertia terms (proportional to $\dot{s}$ and $\ddot{s}$) were neglected and the curvature $H_L$ at the tip of the end cap was unspecified. They already noted that Eq. (18), together with $u_r=\dot{R}$ at $r=R$, implies that

$$\dot{s}=-2\frac{\dot{R}}{R}. \tag{48}$$

It is clear that a long cylinder with rounded end caps which arises in equilibrium when $\dot{s}=0$ cannot arise in dynamic cases in which the coefficient of $L^2-z^2$ is relatively large. $[R(z,t)-R(0,t)]/R(0,t)$ is small where $z^2/L^2$ is small. The variable $z$ enters this theory as a parameter governing the slow variation of $R(z,t)$ near $R(0,t)$. From now on we will write $R(t)$ for $R(z,t)$ when $R(z,t)/R(0,t)\approx 1$.

The curvature $H_L$ in the long cylindrical drop with rounded end caps can be obtained from the exact equilibrium solution, or in the following way. For long drops $J$ approaches from below, so that

$$-\frac{[\![\rho]\!]\Omega^2R_\infty^3}{T}=4, \tag{49}$$

where $R_\infty$ is the large time or equilibrium value of $R(0,t)$, and Eq. (47) reduces to

$$-\frac{T}{R}=-\frac{[\![\rho]\!]\Omega^2R^2}{2}-2H_LT=\frac{2T}{R}-2H_LT. \tag{50}$$

Hence

$$2H_L=\frac{3}{R}. \tag{51}$$

We now adopt the hypothesis that Eq. (51) holds not only in equilibrium, but also during the extensional motion. After combining Eqs. (47), (48), and (51), we get

$$\frac{2T}{R} + [\![\zeta - \sigma]\!] + \frac{[\![\rho]\!]}{2}\Omega^2 R^2 = [\![\rho]\!]\left[\frac{R\ddot{R}}{2} - \left(\frac{3\dot{R}^2}{R^2} - \frac{\ddot{R}}{R}\right)(L^2 - z^2)\right]. \quad (52)$$

We may relate $R$ and $L$ through the conservation of volume of long drops. Then, with a small error, we have

$$R^2 L = R_\infty^2 L_\infty, \quad (53)$$

where $L_\infty$ and $R_\infty$ is the length and radius of the equilibrium drop. Equations (51) and (52) are central results of our analysis. We shall see that when appropriate and fully general constitutive models are used to express $\zeta$ and $\sigma$ in terms of Eq. (47), Eq. (52) is a differential equation for the drop radius.

## IX. NEWTONIAN FLUIDS

In the case of a Newtonian fluid,

$$\zeta = 2\mu\dot{s} = -4\mu\frac{\dot{R}}{R}$$

and

$$\sigma = -\mu\dot{s} = 2\mu\frac{\dot{R}}{R}.$$

If both fluids are Newtonian, then

$$[\![\zeta - \sigma]\!] = -3[\![\mu]\!]\dot{s} = -6[\![\mu]\!]\frac{\dot{R}}{R}. \quad (54)$$

After combining Eqs. (53) and (54) with Eq. (52), we get

$$1 - \frac{3[\![\mu]\!]}{T}\dot{R} + \frac{[\![\rho]\!]\Omega^2 R^3}{4T} = \frac{[\![\rho]\!]}{2T}\left[\frac{R^2\ddot{R}}{2} - \left(\frac{3\dot{R}^2}{R} - \ddot{R}\right)\left(\frac{L_\infty^2 R_\infty^4}{R^4} - z^2\right)\right], \quad (55)$$

which is a nonlinear ordinary differential equation for $R(t,z)$ where $z$ is a parameter. We may write Eq. (55) in terms of dimensionless variables:

In this case, which can be achieved for large values of $\Omega$, we get $[\![\mathbf{t}\cdot\mathbf{Tn}]\!] \approx 0$ everywhere but at the end caps where $\sin\alpha\cos\alpha \neq 0$. The pressure in Eq. (46) may be eliminated using Eq. (40):

$$-\frac{T}{R} + [\![\zeta - \sigma]\!] + \frac{[\![\rho]\!]}{2}(\dot{s}^2 + \ddot{s})(L^2 - z^2)$$

$$= \frac{[\![\rho]\!]}{2}\left(\frac{\dot{s}^2}{4} - \frac{\ddot{s}}{2} - \Omega^2\right)R^2 - 2H_L T. \tag{47}$$

This equation was obtained by Hsu and Flumerfelt (1975) except that inertia terms (proportional to $\dot{s}$ and $\ddot{s}$) were neglected and the curvature $H_L$ at the tip of the end cap was unspecified. They already noted that Eq. (18), together with $u_r = \dot{R}$ at $r = R$, implies that

$$\dot{s} = -2\frac{\dot{R}}{R}. \tag{48}$$

It is clear that a long cylinder with rounded end caps which arises in equilibrium when $\dot{s} = 0$ cannot arise in dynamic cases in which the coefficient of $L^2 - z^2$ is relatively large. $[R(z,t) - R(0,t)]/R(0,t)$ is small where $z^2/L^2$ is small. The variable $z$ enters this theory as a parameter governing the slow variation of $R(z,t)$ near $R(0,t)$. From now on we will write $R(t)$ for $R(z,t)$ when $R(z,t)/R(0,t) \approx 1$.

The curvature $H_L$ in the long cylindrical drop with rounded end caps can be obtained from the exact equilibrium solution, or in the following way. For long drops $J$ approaches from below, so that

$$-\frac{[\![\rho]\!]\Omega^2 R_\infty^3}{T} = 4, \tag{49}$$

where $R_\infty$ is the large time or equilibrium value of $R(0,t)$, and Eq. (47) reduces to

$$-\frac{T}{R} = -\frac{[\![\rho]\!]\Omega^2 R^2}{2} - 2H_L T = \frac{2T}{R} - 2H_L T. \tag{50}$$

Hence

$$2H_L = \frac{3}{R}. \tag{51}$$

We now adopt the hypothesis that Eq. (51) holds not only in equilibrium, but also during the extensional motion. After combining Eqs. (47), (48), and (51), we get

$$\frac{2T}{R} + [\![\zeta - \sigma]\!] + \frac{[\![\rho]\!]}{2}\Omega^2 R^2 = [\![\rho]\!]\left[\frac{R\ddot{R}}{2} - \left(\frac{3\dot{R}^2}{R^2} - \frac{\ddot{R}}{R}\right)(L^2 - z^2)\right]. \quad (52)$$

We may relate $R$ and $L$ through the conservation of volume of long drops. Then, with a small error, we have

$$R^2 L = R_\infty^2 L_\infty, \quad (53)$$

where $L_\infty$ and $R_\infty$ is the length and radius of the equilibrium drop. Equations (51) and (52) are central results of our analysis. We shall see that when appropriate and fully general constitutive models are used to express $\zeta$ and $\sigma$ in terms of Eq. (47), Eq. (52) is a differential equation for the drop radius.

## IX. NEWTONIAN FLUIDS

In the case of a Newtonian fluid,

$$\zeta = 2\mu\dot{s} = -4\mu\frac{\dot{R}}{R}$$

and

$$\sigma = -\mu\dot{s} = 2\mu\frac{\dot{R}}{R}.$$

If both fluids are Newtonian, then

$$[\![\zeta - \sigma]\!] = -3[\![\mu]\!]\dot{s} = -6[\![\mu]\!]\frac{\dot{R}}{R}. \quad (54)$$

After combining Eqs. (53) and (54) with Eq. (52), we get

$$1 - \frac{3[\![\mu]\!]}{T}\dot{R} + \frac{[\![\rho]\!]\Omega^2 R^3}{4T} = \frac{[\![\rho]\!]}{2T}\left[\frac{R^2\ddot{R}}{2} - \left(\frac{3\dot{R}^2}{R} - \ddot{R}\right)\left(\frac{L_\infty^2 R_\infty^4}{R^4} - z^2\right)\right], \quad (55)$$

which is a nonlinear ordinary differential equation for $R(t,z)$ where $z$ is a parameter. We may write Eq. (55) in terms of dimensionless variables:

$$\eta(t,z) = \frac{R}{R_\infty},$$

$$\xi = \frac{z}{L_\infty},$$

$$\tau = t\Omega, \tag{56}$$

where

$$\frac{[\rho]\Omega^2 R_\infty^3}{4T} = -1. \tag{57}$$

Thus

$$1 - \lambda\dot{\eta} - \eta^3 = -\eta^2\ddot{\eta} + 2\frac{L_\infty^2}{R_\infty^2}\left(\frac{3\dot{\eta}^2}{\eta} - \ddot{\eta}\right)\left(\frac{1}{\eta^4} - \xi^2\right), \tag{58}$$

where

$$\lambda = \frac{3[\mu]\Omega R_\infty}{T}.$$

The right-hand side of Eq. (58) arises from the inertia terms, the terms proportional to $\rho$ in Eq. (32) and (33).

If the inertia is neglected, then Eq. (58) reduces to

$$1 - \lambda\dot{\eta} - \eta^3 = 0, \tag{59}$$

with an initial condition

$$\eta(0) = \eta_0 = R_0/R_\infty. \tag{60}$$

This ordinary differential equation can be integrated exactly to get an implicit solution for $\eta$:

$$-\frac{1}{6}\log\left(\frac{1-2\eta+\eta^2}{1-2\eta_0+\eta_0^2}\frac{1+\eta_0+\eta_0^2}{1+\eta+\eta^2}\right) + \frac{1}{\sqrt{3}}\left[\tan^{-1}\left(\frac{2\eta+1}{\sqrt{3}}\right) - \tan^{-1}\left(\frac{2\eta_0+1}{\sqrt{3}}\right)\right] = \frac{t}{\lambda\Omega}. \tag{61}$$

It is probable that the various assumptions which are required for the validity of Eq. (59) are most valid near equilibrium. We may treat this case exactly in an asymptotic regime linearized around the equilibrium solution for the long cylindrical drop, $J = 4$, $R = R_\infty, L_\infty > 4R_\infty$. We substitute $\eta = 1 + \epsilon$ for small $\epsilon$ into Eq. (58) and find that

$$\lambda\dot{\epsilon} + 3\epsilon - \theta\ddot{\epsilon} = 0, \tag{62}$$

where

$$\theta = 2\frac{L_\infty^2}{R_\infty^2}(1 - \xi^2) + 1. \tag{63}$$

We may always find a relaxing solution proportional to $e^{-mt}$ with a positive

$$m = -\frac{\lambda}{2\theta} \pm \sqrt{\frac{\lambda^2}{4\theta^2} + \frac{3}{\theta}}, \tag{64}$$

where $+$ is chosen when $\lambda > 0 (\llbracket\mu\rrbracket > 0)$ and $-$ is chosen when $\lambda < 0 (\llbracket\mu\rrbracket < 0)$. When $|\lambda| \gg \theta$, a typical case, then

$$m = \frac{3}{|\lambda|} = \frac{T}{\llbracket\mu\rrbracket \Omega R_\infty}. \tag{65}$$

We may express the exponent $m$ in terms of given parameters, eliminating $R_\infty$ with Eq. (49),

$$m = \left(\frac{T^2 \Delta\rho}{4\Omega}\right)^{1/3} \frac{1}{\Delta\mu}, \tag{66}$$

where $\Delta\rho = |\llbracket\rho\rrbracket|, \Delta\mu = |\llbracket\mu\rrbracket|$ are positive. The approach to equilibrium is very slow when the viscosity difference is large. According to the present theory, the expansion of the drop in liquids of matched viscosity $\llbracket\mu\rrbracket = 0$ is entirely determined by inertia with $m = \sqrt{3/\theta}$.

The rejection of growing solutions with a negative $m$ is actually not justified on mathematical grounds. We can regard Eq. (62) as a stability equation, albeit in a severely restricted class of strictly extensional flow. If we adopt this point of view we shall be obliged to say that the equilibrium is always unstable, since the stability problem gives rise to growing modes. This conclusion is at variance with results of exact analysis of the stability of equilibrium, done without assuming pure extension, which was discussed at the end of Sec. V. When we discard

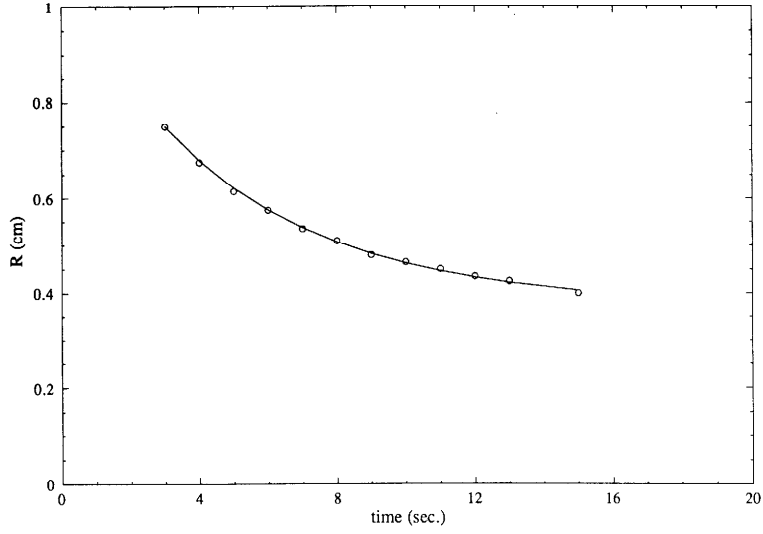


**FIG. 12.** Comparison of Eq. (61) with the data from Hsu and Flumerfelt (1975), Fig. 4, with $T = 22.6$ dyn/cm, $[\![\mu]\!] = 7500$ P, $-[\![\rho]\!] = 0.31$ g/cm$^3$, $\Omega = 2440$ rpm, and $R_0 = 0.75$ cm.

growing roots we are doing something physical, which may be wrong and it is necessary to exercise caution, as the following observation clearly shows. Suppose $\theta = 0$. Then

$$\lambda\dot{\epsilon} + 3\epsilon = 0 \tag{67}$$

and

$$\epsilon(t) = \epsilon(t_0)e^{-m(t-t_0)}, \tag{68}$$

where $m$ is given by Eq. (65). If $[\![\mu]\!] > 0$ we have exponential decay and if $[\![\mu]\!] < 0$ we have exponential growth. We may conclude from this that the Hsu–Flumerfelt assumption of extensional approach to equilibrium is not possible when the light fluid in the drop is less viscous than the ambient or outside fluid, $\mu_2 > \mu_1$.

It is probably most efficient to test the various predictions of this theory which is based on the Hsu–Flumerfelt assumption of purely extensional flow by a direct numerical simulation. Such a simulation is presently under way. Next we turn to experimental tests of the theory.

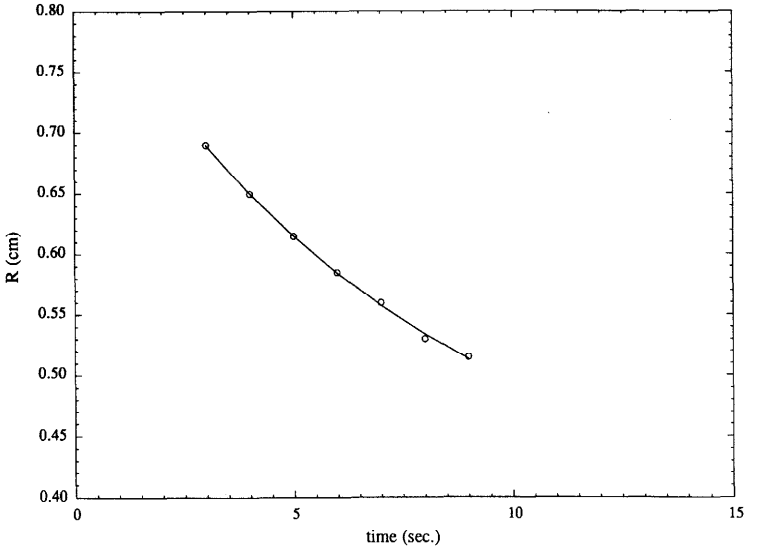


**FIG. 13.** Comparison of Eq. (61) with the data from Hsu and Flumerfelt (1975), Table I, with $T = 22.6$ dyn/cm, $[\mu] = 7500$ P, $[\rho] = -0.31$ g/cm$^3$, $\Omega = 2130$ rpm, and $R_0 = 0.69$ cm.

It should be noted that Eq. (67) and its solution (68) lead to the decaying exponential formula given by Eq. (13). However, the relaxation times $m$ predicted by Eq. (66) do not agree with the actually observed relaxation times.

## X. COMPARISON WITH EXPERIMENTS

The transient theory for Newtonian liquids presented in Sec. IX is in a satisfactory agreement with experiment only in limited time intervals and not for the entire transient of drop expansion after a step increase of angular velocity, even if the short period in which inertia may be important is discarded. Hsu and Flumerfelt (1975) gave experimental data for a two fluid system of Cannon ASTM standard oil $[\rho,\mu] = (0.91$ g/cm$^3$, 7500 P) and aqueous glycerol $[\rho,\mu] = (1.26$ g/cm$^3$, 0.5 P) with an interfacial tension of 22.6 dyn/cm. They presented their data for relaxation at $\Omega = 2130$ rpm in their Table I and $\Omega = 2440$ rpm in their Fig. 4. They restricted the data in their table to $t > 3$ s to avoid the effects of inertia. They also restricted their data to $t < 16$ s to avoid

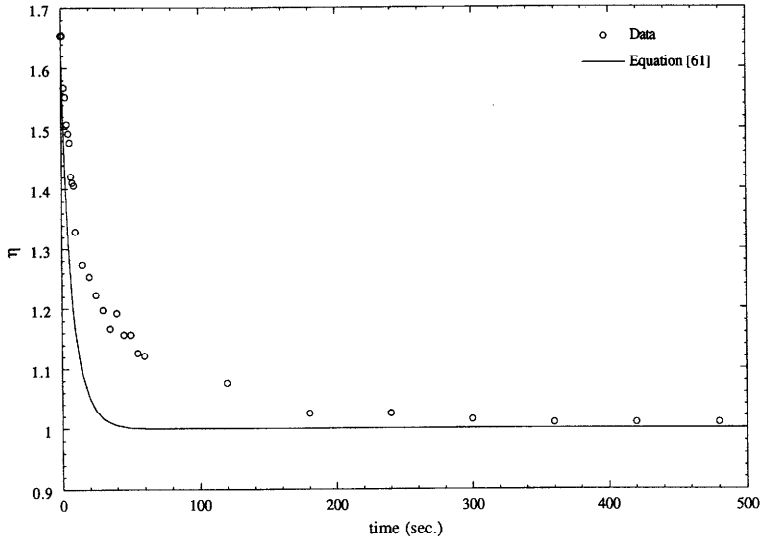


**FIG. 14.** Comparison of Eq. (61) with 100 000 cs PDMS in glycerol, with $T = 32.3$ dyn/cm, $[\mu] = 973.5$ P, $[\rho] = -0.286$ g/cm$^3$, $\Omega = 3208$ rpm, and $R_0 = 0.263$ cm.

interfacial effects and they identified the interval $3 \text{ s} < t < 16$ s as one where centrifugal and viscous forces dominate so that $\lambda\dot{\eta} + \eta^3 = 0$ approximately. We have presented data from their Fig. 4 in our Fig. 12, omitting data points with $t < 3$ s. The data from their Table 1 is shown in our Fig. 13. Their data is fitted to the initial point of the equation at $t = 3$ s. Satisfactory agreement between theory and experiments are found in the limited range of time where inertial and interfacial effects are both negligible.

If we try to account for interfacial effects, using Eq. (61), the agreement with experiments disappears. If the correct surface tension 32.3 dyn/cm is used and agreement with equilibrium, $\eta = 1$, is forced, then the experimental points do not fit Eq. (61). This is seen clearly in Fig. 14, which gives data from our experiments. The same magnitude of discrepancies between theory and experiment occurs when fitting the data of Hsu and Flumerfelt (1975) with Eq. (61). It appears that it is not possible to use the Hsu–Flumerfelt idea of pure extension to obtain interfacial tension.

## XI. VISCOELASTIC FLUIDS

Returning now to the viscoelastic fluid (23), we note that for steady extension, $\dot{s}$ is independent of time,

$$\mathbf{A}_n = \mathbf{A}_1^n \tag{69}$$

is independent of time, and

$$\mathbf{C}_t(\tau) = \exp[-\mathbf{A}_1(t-\tau)]. \tag{70}$$

It follows then from the Frechet expansion [see Eqs. (16.46) in Joseph (1990)] that

$$\mathbf{S} = \overset{t}{\underset{\tau=-\infty}{F}} \exp[(\tau - t)\mathbf{A}_1] = \mathbf{f}(\mathbf{A}_1), \tag{71}$$

where $F(\cdot)$ is an isotropic, symmetric tensor valued function. Such tensor functions may be represented by quadratic polynomials in $\mathbf{A}_1$ with scalar coefficients that depend on the invariants of $\mathbf{A}_1$. Since $\mathrm{tr}(\mathbf{A}_1) = 0$ for incompressible fluids there are two active invariants

$$\mathrm{II} = \tfrac{1}{2}[(\mathrm{tr}\,\mathbf{A}_1)^2 - \mathrm{tr}(\mathbf{A}_1^2)], \tag{72}$$

$$\mathrm{III} = \det \mathbf{A}_1$$

and after absorbing terms proportional to $\mathbf{1}$ in the pressure, we get

$$\mathbf{S} = \mathbf{f}(\mathbf{A}_1) = g(\mathrm{II},\mathrm{III})\mathbf{A}_1 + h(\mathrm{II},\mathrm{III})\mathbf{A}_1^2. \tag{73}$$

It follows now that if the flow is extensional at all times past, then the present value of the stress must be determined by the history of a quadratic polynomial like (73). A "linear" viscoelastic theory of unsteady extensional flow can be framed as a Boltzmann type integral, linear in $\mathbf{f}$:

$$\mathbf{S} = \int_{-\infty}^{t} [g(\mathrm{II},\mathrm{III},t-\tau)\mathbf{A}_1(\tau) + h(\mathrm{II},\mathrm{III},t-\tau)\mathbf{A}_1^2(\tau)]\,d\tau, \tag{74}$$

where

$$\text{II} = -3\dot{s}^2 = -12\frac{\dot{R}^2}{R^2},$$

$$\text{III} = 2\dot{s}^3 = -16\frac{\dot{R}^3}{R^3}. \tag{75}$$

In the present study of relaxation $\dot{R}\to 0$. If $\dot{R}\neq 0$ is constant, then we are in the frame of steady elongational flow. This kind of flow has been studied intensively by rheologists for many years but is not easy to realize in practice. If it could be realized then $\mathbf{A}_1$ would be independent of $\tau$ and Eq. (74) would reduce to Eq. (73) with

$$g(\text{II},\text{III}) = \int_{-\infty}^{t} g(\text{II},\text{III},t-\tau)d\tau, \tag{76}$$

$$h(\text{II},\text{III}) = \int_{-\infty}^{t} h(\text{II},\text{III},t-\tau)d\tau. \tag{77}$$

The components of $\mathbf{S}$ in cylindrical coordinates in the steady case are

$$[\mathbf{S}] = \begin{bmatrix} \sigma & 0 & 0 \\ 0 & \psi & 0 \\ 0 & 0 & \xi \end{bmatrix} = \begin{bmatrix} -g\dot{s}+h\dot{s}^2 & 0 & 0 \\ 0 & -gs+h\dot{s}^2 & 0 \\ 0 & 0 & 2g\dot{s}+4h\dot{s}^2 \end{bmatrix}. \tag{78}$$

Hence, the canonical expression for the extensional viscosity in pure steady cylindrical extension is given by

$$\xi - \sigma = 3[g(\text{II},\text{III})\dot{s} + h(\text{II},\text{III})\dot{s}^2]. \tag{79}$$

The extensional viscosity is the coefficient of $\dot{s}$ in Eq. (79). It is of interest to expand Eq. (79) up to terms of order $\dot{s}^2$. This expansion can be carried out in general [see Eq. (13) in Chap. 17 of Joseph (1990)] without assuming extensional flow. After evaluating the general second order expansion or extensional flow we find that

$$\xi - \sigma = 3\dot{s}\mu + 3(\alpha_1+\alpha_2)\dot{s}^2 + O(\dot{s}^3), \tag{80}$$

where $\mu$ is the zero shear viscosity and $\alpha_1$, $\alpha_2$ are the quadratic correction coefficients for second order fluids, sometimes called Rivlin–Ericksen constants. We may therefore conclude that

$$\mu = g(0,0) = \int_{-\infty}^{t} g(0,0,t,-\tau)d\tau \tag{81}$$

and

$$\alpha_1 + \alpha_2 = h(0,0) = \int_{-\infty}^{t} h(0,0,t,-\tau)d\tau. \tag{82}$$

In the unsteady case, we find that

$$\begin{bmatrix} \sigma(t) & 0 & 0 \\ 0 & \psi(t) & 0 \\ 0 & 0 & \zeta(t) \end{bmatrix}$$

$$= \int_{-\infty}^{t} \begin{bmatrix} -g\dot{s} + h\dot{s}^2 & 0 & 0 \\ 0 & -g\dot{s} + h\dot{s}^2 & 0 \\ 0 & 0 & 2g\dot{s} + 4h\dot{s}^2 \end{bmatrix} d\tau, \tag{83}$$

where, under the integral, $\dot{s} = -2\dot{R}(\tau)/R(\tau)$ and the invariants II and III are given by Eq. (75). Using Eqs. (79) and (48), we may write Eq. (52) as

$$1 + \frac{[\![\rho]\!]\Omega^2 R^3}{4T} - \frac{3R}{T}\int_{-\infty}^{t}\left([\![g]\!]\frac{\dot{R}(\tau)}{R(\tau)} - 2[\![h]\!]\frac{\dot{R}^2(\tau)}{R^2(\tau)}\right)d\tau$$

$$= \frac{[\![\rho]\!]R^2\ddot{R}}{4T} - \frac{[\![\rho]\!]L_\infty^2}{2T}\left(\frac{3\dot{R}^2}{R} - \ddot{R}\right)\left(\frac{R_\infty^4}{R^4} - \frac{z^2}{L_\infty^2}\right), \tag{84}$$

where

$$[\![g]\!] = g_1(\mathrm{II},\mathrm{III},t-\tau) - g_2(\mathrm{II},\mathrm{III},t-\tau)$$

and

$$[\![h]\!] = h_1(\mathrm{II},\mathrm{III},t-\tau) - h_2(\mathrm{II},\mathrm{III},t-\tau)$$

are functions of $R(\tau)$ by Eq.(75). Equation (84) is an integrodifferential equation for $R(\tau)$.

Equation (84) can be used to interpret relaxation curves in spinning drop devices in terms of to-be-determined rheometrical functions $g$ and $h$ which characterize unsteady extensional flow. Each choice of $g$ and $h$ gives rise to an explicit equation for the radius $R(t)$ of the drop. Steady extension cannot be attained in spinning drop devices, so that we are

looking at a somewhat unconventional but possible more practical problem than usual. In practice, various simplified forms of $g$ and $h$ would be required to integrate Eq. (84) and to interpret results of experiments.

It is possible that the various assumptions which are required for the validity of Eq. (84) are most valid near equilibrium. (This does not, however, appear to be true in the Newtonian case in which the decay constant for the extensional theory does agree with measurements.) We may treat this case exactly in an asymptotic regime linearized around the equilibrium solution for the long cylindrical drop, $J = 4$, $R = R_\infty$, $L_\infty > 4R_\infty$. We write $R = R_\infty + \delta$ and linearize to find that

$$\frac{3}{T}\int_{-\infty}^{t} [\![g(0,0,t-\tau)]\!]\frac{d\delta}{d\tau}\,d\tau + 3\frac{\delta}{R_\infty} - \frac{\theta}{R_\infty}\frac{d^2\delta}{dt^2} = 0. \tag{85}$$

It is perhaps useful for a first try to express the relaxation kernel as simple exponentials with a single time of relaxation

$$[\![g(0,0,t-\tau)]\!] = G_1 \exp\left(-\frac{t-\tau}{\lambda_1}\right) - G_2 \exp\left(-\frac{t-\tau}{\lambda_2}\right), \tag{86}$$

with constants $G_1$, $G_2$, $\lambda_1$, $\lambda_2$. We may seek relaxing solutions of Eqs. (85) and (86),

$$\frac{\delta}{R_\infty} = C\exp(-mt), \tag{87}$$

with a positive $m$ satisfying

$$-\frac{3mR_\infty}{T}\left[\!\!\left[\frac{G}{(1/\lambda)-m}\right]\!\!\right] + 3 - \theta m^2 = 0. \tag{88}$$

Equation (88) implicitly gives the relaxation function for viscoelastic fluids. We can suppose, as before with Eq. (66), that $\theta = 0$. Then, instead of Eq. (88), we get

$$-3mR_\infty\left[\!\!\left[\frac{G}{(1/\lambda)-m}\right]\!\!\right] + 3 = 0. \tag{89}$$

Solving this for $m$ we get

$$m = \left( \frac{-\lambda_1 - AG_1\lambda_1 - \lambda_2 + AG_2\lambda_2}{\lambda_1\lambda_2 + AG_1\lambda_1\lambda_2 - AG_2\lambda_1\lambda_2} \right) \pm \frac{1}{2}\sqrt{\frac{(-\lambda_1 - AG_1\lambda_1 - \lambda_2 + AG_2\lambda_2)^2}{(\lambda_1\lambda_2 + AG_1\lambda_1\lambda_2 - AG_2\lambda_1\lambda_2)^2} - \frac{4}{(\lambda_1\lambda_2 + AG_1\lambda_1\lambda_2 - AG_2\lambda_1\lambda_2}}, \tag{90}$$

where $A = 3R_\infty/T$. This formula has not yet been tested by experiments.

## XII. CONCLUSIONS

We have developed an instrument for measuring interfacial tension and rheological properties of polymer blends. A data reduction scheme based on a theoretically motivated procedure of exponential fitting in Eq. (13) was implemented and shown to yield accepted values of interfacial tension in reduced time. The decay rate has yet to be determined from analysis. A global theory of relaxation assuming pure unsteady extension superposed on rigid rotation, following ideas of Hsu and Flumerfelt was developed for Newtonian and non-Newtonian fluids. This theory works well in a rather limited range of parameters.

## ACKNOWLEDGMENTS

This work was supported by the Department of Energy, the National Science Foundation, the Hoechst-Celanese Corporation, the Army High Performance Computational Research Center, and the Army Research Office, Mathematics. We would like to thank Uttandaraman Sundararaj, Department of Chemical Engineering and Material Science, University of Minnesota, Minneapolis, for providing the zero shear viscosity measurements of our polymers.

## References

Anastasiadis, S. H., J. K. Chen, J. T. Koberstein, J. E. Sohn, and J. A. Emerson, "The determination of polymer interfacial tension by drop image processing: comparison of theory and experiment for the pair, poly(dimethyl siloxane)/polybutadiene," Polym. Eng. Sci. **26**, 1410 (1986).

Arney, M. S., "Selected Topics in the Mechanics of Two-Fluid Systems," Ph.D. thesis, University of Minnesota, Minneapolis, Minnesota, 1992.

Carriere, C. J., A. Cohen, and C. B. Arends, "Estimation of interfacial tension using shape evolution of short fibers," J. Rheol. **33**, 681 (1989).

Carriere, C. J. and A. Cohen, "Evaluation of the interfacial tension between high molecular weight polycarbonate and PMMA resins with the imbedded fiber retraction technique," J. Rheol. **35**, 205 (1991).

Chappelear, D. C., "Interfacial tension between molten polymers," Polym. Prepr. **5**, 363 (1964).

Dealy, J. J. and K. F. Wissbrun, *Melt Rheology and its Role in Plastics Processing* (Van Nostrand Reinhold, New York, 1990).

Elemans, P. H. M., J. M. H. Jannssen, and H. E. H. Meijer, "The measurement of interfacial tension in polymer/polymer systems: The breaking thread method," J. Rheol. **34**, 1311 (1990).

Elmendorp, J. J., Ph.D. thesis, Delft University of Technology, 1986.

Elmendorp, J. J. and G. De Vos, "Measurement of interfacial tensions of molten polymer systems by means of the spinning drop method," Polym. Eng. Sci. **26**, 415 (1986).

Elmendorp, J. J., "A study on polymer blending microrheology," Polym. Eng. Sci. **25**, 1041 (1985).

Elmendorp, J. J., M. de Wit, and B. Ouderhaarlem, "Een oppervlaktespanningsmeter voor polymeersmelten," Mikronick. **28**, 9 (1988).

Fayt, R., R. Jerome, and Ph. Tessie', "Characterization and control of interfaces in emulsified incompatible polymer blends," Polym. Eng. Sci. **27**, 328 (1987).

Gaylord, N. G., "Compatibilizing agents: Structure and function in polyblends," J. Macromol. Sci.-Chem. A **26**, 1211 (1989).

Gergen, W. P., S. Davison, and R. G. Lutz, "Thermoplastic elastomer IPN's," Rubber Chem. Technol. **58**, 857 (1985).

Hsu, J. C. and R. W. Flumerfelt, "Rheological applications of a drop elongation experiment," Trans. Soc. Rheol. **19**, 523–540 (1975).

James, S., J. Scatzle, and P. Navard, paper given at Sixth Annual Meeting of Polymer Processing Society, Nice, April, 1990.

Joseph, D. D., M. S. Arney, and G. Ma, "Upper and lower bounds for interfacial tension using spinning drop devices," J. Colloid Interface Sci. **148**, 291 (1992).

Joseph, D. D. and L. Preziosi, "Stability of rigid motions and coating films in bicomponent flows of immiscible liquids," J. Fluid Mech. **185**, 323–351 (1987).

Joseph, D. D., *Stability of Fluid Motions II*, Springer-Verlag Tracts in Natural Philosophy (Springer, Berlin, 1976).

Joseph, D. D., *Fluid Dynamics of Viscoelastic Liquids*, Springer Series in Applied Mathematical Sciences (Springer, Berlin, 1990), Vol. 84.

Joseph, D. D. and D. Hultman, U.S. Patent application, serial No. 07/742,291 (1991).

Laun, H. M. and H. Schuch, "Transient elongational viscosities and drawability of polymer melts," J. Rheol. **33**, 119 (1989).

Patterson, H. T., K. H. Hu, and T. H. Grindstaff, "Measurement of Interfacial and Surface Tensions in Polymer Systems," J. Polym. Sci. C **34**, 31 (1971).

Press, W. H., B. P. Flannery, S. A. Teukolsky, and W. T. Veterling, *Numerical Recipes* (Cambridge University Press, Cambridge, 1986), p. 294ff.

Princen, H. M., I. Y. Z. Zia, and S. G. Mason, "Measurement of Interfacial Tension from the Shape of the Rotating Drop," J. Colloid Interface Sci. **23**, 99–107 (1967).

Roe, R. J., "Surface Tension of Polymer Liquids," J. Phys. Chem. **72**, 2013 (1968).

Shih, C. K., "Fundamentals of Polymer Compounding—Part II: Simulation of Polymer Compounding Process," ANTEC '91, 99 (1991).

Than, P., L. Preziosi, D. D. Joseph, and M. S. Arney, "Measurement of Interfacial Tension Between Immiscible Liquids with the Spinning Rod Tensiometer," J. Colloid Interface Sci. **124**, 552–559 (1988).

Tomotika, S., "On the instability of a cylindrical thread of a viscous liquid surrounded by another viscous fluid," Proc. R. Soc. London Ser. A **150**, 332 (1935).

Verdier, C.,"Topics in the Fluid Mechanics of Viscoelastic Liquids," Ph.D. dissertation, Department of Aerospace Engineering and Mechanics, University of Minnesota, Minneapolis, Minnesota, 1990.

Vonnegut, B., "Rotating Bubble Method for the Determination of Surface and Interfacial Tension," Rev. Sci. Instrum. **13**, 6–9 (1942).

Wu, S., "Formation of dispersed phase in incompatible polymer blends: Interfacial and rheological effects," Polym. Eng. Sci. **27**, 335 (1987).

Wu, S., "Interfacial and surface tensions of polymers," J. Macromol Sci.—Rev. Macromol. Chem. C **10**, 1 (1974).

Wu, S., "Surface and interfacial tensions of polymer melts I. Polyethylene, polysiobutylene, and polyvinyl acetate," J. Colloid Interface Sci. **31**, 153 (1969).

Xanthos, M., "Interfacial agents for multiphase polymer systems: Recent advances," Polym. Eng. Sci. **28**, 1392 (1988).